Predication of Steady-State Thermal Characteristics of a Resistance Spot Welding Transformer in Battery Manufacturing Application

Armin Saki, Saleh Rahmani, Masoud Yavarinasab, Hossein Abootorabi Zarchi, *Senior Member, IEEE*, Salman Abdi, *Senior Member, IEEE*, Sérgio M. A. Cruz, *Senior Member, IEEE*, and Hamidreza Mosaddegh-Hesar, *Member, IEEE*

***Abstract*—This article introduces a novel finite-element-method-based model designed to analyze the electromagnetic–thermal dynamics of resistance spot welding (RSW) transformers used in battery manufacturing. The RSW process, inherently multiphysics and sensitive to temperature fluctuations, involves phase changes within the metal materials. This complexity, combined with frequent electrode connections and disconnections during welding (variable structure), renders traditional steady-state analysis methods inadequate for accurately capturing temperature and electromagnetic parameters under thermal steady-state conditions, and the effect of changing power electronics parameters (frequency, number of cycles, and firing angle) on continuous operation is also unpredictable. The article proposes a method capable of determining temperature trends during electrode opening (rest period). It simplifies the temperature characteristics and material properties of the welding spot. These variations are equated and simplified as a constant temperature and an equivalent material, respectively. The proposed model, rooted in finite-element analysis and experimentally validated, enables a bidirectional electromagnetic–thermal simulation through steady-state thermal analysis. This simulation generates results for temperature and electromagnetic values during steady-state operation, demonstrating close agreement with experimental results. Consequently, the developed model showcases its capability in predicting the impacts and sensitivities of various factors, such as voltage cycle number, firing angle, and rest period duration within the RSW process.**

Manuscript received 3 March 2024; revised 13 June 2024; accepted 10 July 2024. This work was supported by the Portuguese Foundation for Science and Technology—Fundação para a Ciência e Tecnologia, I.P. under Grant 10.54499/UIDB/50008/2020. Recommended for publication by Associate Editor W. Huang. *(Corresponding author: Hossein Abootorabi Zarchi.)*

Armin Saki is with the Sun-Air Research Institute, Ferdowsi University of Mashhad, Mashhad 9177948974, Iran, and also with the Faculty of Engineering, Department of Electrical Engineering, Ferdowsi University of Mashhad, Mashhad 9177948974, Iran (e-mail: armin.saki@mail.um.ac.ir).

Saleh Rahmani and Masoud Yavarinasab are with the Sun-Air Research Institute, Ferdowsi University of Mashhad, Mashhad 9177948974, Iran (e-mail: salehrahmani@um.ac.ir; yavarinasab@um.ac.ir).

Hossein Abootorabi Zarchi and Hamidreza Mosaddegh-Hesar are with the Faculty of Engineering, Department of Electrical Engineering, Ferdowsi University of Mashhad, Mashhad 9177948974, Iran (e-mail: abootorabi@um.ac.ir; hamid.mosaddegh@alumni.um.ac.ir).

Salman Abdi is with the School of Engineering, University of East Anglia, NR4 7TJ Norwich, U.K. (e-mail: s.abdi-jalebi@uea.co.uk).

Sérgio M. A. Cruz is with the Department of Electrical and Computer Engineering and the Instituto de Telecomunicações, University of Coimbra, 3030-290 Coimbra, Portugal (e-mail: smacruz@deec.uc.pt).

Color versions of one or more figures in this article are available at https://doi.org/10.1109/TPEL.2024.3429450.

Digital Object Identifier 10.1109/TPEL.2024.3429450

***Index Terms*—Electromagnetic–thermal analysis, finite-element method (FEM), resistance spot welding (RSW), thermal steady-state conditions, welding transformer (WT).**

I. Introduction

RESISTANCE spot welding (RSW) is an industrial process that welds metal plates by the circulation of a high current through the secondary of a step-down transformer. Widely employed in the welding industry for joining metal sheets and parts, RSW plays a pivotal role in vehicle body assembly [1]. During the welding process, two electrodes compress metal sheets, typically driven by air pressure in a pneumatic cylinder, servo actuator, or hydraulic system. Thermal energy is introduced into the system through a step-down welding transformer (WT) [2]. The WT under investigation operates with a single-phase ac power supply. It utilizes two silicon controlled rectifiers (SCRs) or thyristors connected in parallel, where one conducts current during the positive half-cycle and the other during the negative half-cycle. In Fig. 1, the model of a step-down WT is depicted, where L_1 and R_1 represent the equivalent leakage reactance and resistance of the primary winding, while L_2 and R_2 denote those in the secondary winding [5], [6]. The control of the welding process involves adjusting the firing angle, also known as the trigger time, of each SCR alternately for each control cycle. The firing angle values, ranging from 0° to 180°, linearly correspond to fire times between 0 and 10 ms, for a 50 Hz supply frequency.

Typically, the welding cycle generates current by modulating several voltage cycles with specific firing angles to achieve the required energy transfer. A complete welding cycle comprises an incremental ramp (gradual increase in the firing angle over multiple cycles), cycles with the desired firing angle, and, in some cases, a decremental ramp (gradual decrease of the firing angle over several cycles). Fig. 2 shows the general scheme depicting the voltage and current patterns of the WT.

In traditional transformers, a continuous supply voltage is applied to the primary winding without variable structures or phase changes in the materials connected to the secondary side. Consequently, the transformer temperature increases steadily until reaching a steady-state value. In such cases, electromagnetic–thermal modeling and loss mapping simulation of the transformer, treating it as a heat source, can be employed to obtain transient and steady-state temperatures [7], [8], [9], [10],

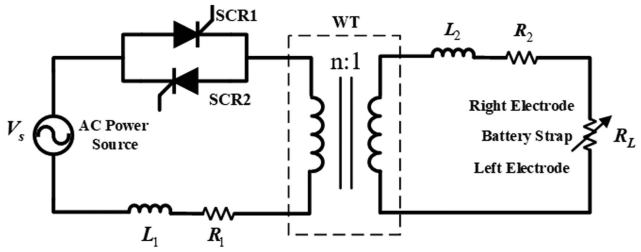

Fig. 1. Welding transformer structure with a single-phase AC power supply.

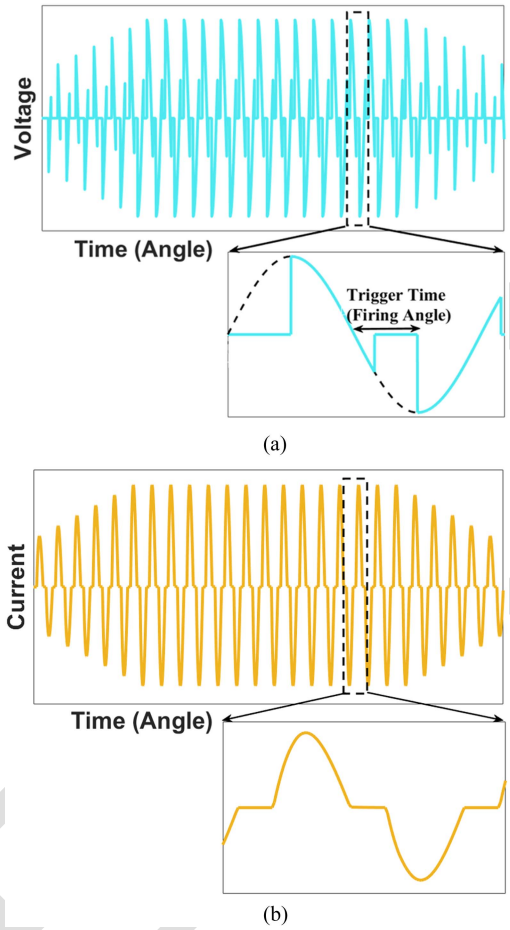

Fig. 2. General representation of voltage and current in a WT: (a) applied voltage and (b) supply current.

[11], [12], [13], [14]. Therefore, a uniform multiphysics simulation is employed to achieve continuous energy conversion between electrical, magnetic, and thermal domains in the electromagnetic–thermal coupling. This approach allows for obtaining both thermal (temperature) and electromagnetic (voltage, current, and magnetic field) results. Due to the inherent stability of the transformer's structure and material phases, the simulation enables continuous transient and steady-state thermal analysis on the fixed structure and materials of the model. Hence, transient and steady-state temperature distributions are obtained, corresponding to transient and steady-state conditions, respectively, in conventional transformers.

However, the RSW transformer brings about complexities due to the intermittent nature of electrode connection throughout the welding process. Moreover, variations in the structure, material composition, and phase at the welding spot add to the inherent variability. Additionally, temperature limitations during the metal melting process—where the material maintains a constant temperature corresponding to its melting point—further complicate the utilization of conventional methods. These distinct characteristics inherent to the RSW process require specialized modeling and simulation approaches to accurately capture its dynamic and temperature-sensitive nature. The accurate prediction of the steady-state temperature in the RSW transformer, serving as a thermal spot-welding source, is crucial due to its highly nonlinear and pulsating operation, impacting various transformer characteristics, such as voltage, current, magnetic field, and operating temperature, of the welding spot and electrode junction.

The existing studies in RSW literature predominantly focus on the temperature rise of the electrodes and the nugget (molten metal at the welding spot) and lack an approach to predict the steady-state temperature across different parts of the transformer. Moreover, these discussions are often limited to specific time periods, typically covering only one or a few welding cycles. Eisazadeh et al. [15] developed a multiphysics finite-element (FE) simulation coupling the RSW phenomenon with the ability to adjust welding parameters. Their model primarily derives nugget growth through a multiphysics analysis involving temperature and welding cycle duration. However, the article does not address the steady-state temperature of the RSW transformer.

In [16], a comparative analysis of three power supply types in the RSW—dc mode, standard sinusoidal, and standard single-phase ac RSW mode adjusted by the firing angle of the SCRs—was conducted. The results of thermal and electrical dynamic resistance analysis were extracted for a limited time span of 14 welding cycles at a frequency of 50 Hz. Notably, this approach did not consider steady-state temperature analysis, where the cycles of welding and rest are frequently repeated. Additionally, the investigation did not encompass the temperature assessment of transformer components, such as windings, core, and frame. Similarly, Xia et al. [17] proposed a finite-element method (FEM)-based multiphysics model for the RSW process, incorporating electrical, thermal, and mechanical coupling. The model was designed to simulate nugget growth and some quantities, including the dynamic resistance. However, the analyses were conducted within limited time intervals of welding cycles, and the steady-state temperature of the transformer was not investigated. Other studies also possess this deficiency [18], [19], [20], [21], [22], [23].

To address these gaps in the existing literature, this article places special emphasis on determining the steady-state temperature of the RSW transformer using multiphysics modeling and simulation. Initially, a method is proposed to track temperature variations during electrode opening, encompassing the rest period or postwelding phase. Subsequently, a novel approach is introduced, equating and simplifying the transient temperature characteristics and material properties of the welding spot load

across the welding cycle. This cycle spans prewelding, welding, and postwelding. The alignment of these factors with a constant temperature and an equivalent material is carefully crafted to ensure a consistent temperature rise in the electrodes.

In the thermal model employed for the two-way electromagnetic–thermal analysis, the temperature of the welding spot is established as equivalent to the determined constant temperature. Subsequently, the electromagnetic model receives the voltage signal encompassing the entire welding cycle. As a result, the electromagnetic (transient) and thermal (steady-state) multiphysics coupling analysis enables the determination of steady-state temperature, voltage, current, and magnetic field exhibited by the RSW transformer during continuous operation. This analysis predicts steady-state temperatures across varying power electronics parameters of the control panel: frequency, welding cycle numbers, welding firing angles, and rest period times. One specific case is compared and validated against experimental results to assess the accuracy and reliability of the proposed model.

Indeed, the conventional methods for common transformers used previously to determine steady-state temperature in RSW transformers were insufficient due to the nonconstant structure, complex, multiphysics, time-dependent, and temperature-dependent nature of the RSW process. On the other hand, previous articles did not address the steady-state temperature of RSW transformer components. In this regard, the innovation of this article is to provide an approach to equalize the spot welding, enabling the determination of the steady-state temperature of transformer components, as well as the electromagnetic characteristics (voltage, current, and magnetic field) at this steady-state temperature. This approach can be extended to other electromagnetic systems and processes with variable material phases and structures that are time- and temperature-dependent.

II. Electromagnetic-Thermal Modeling and Simulation of the RSW Transformer

A. Modeling

The RSW transformer is modeled in three dimensions (3-D). The load of the developed model is the electrical resistance of the welding spot lead considering the hydraulic forces applied to the electrodes. In fact, due to the constant forces during the entire welding process of the battery strap, their effect on the reduction of the electrical resistance of the welding spot has been taken into account. This consideration prompts a two-way multiphysics analysis conducted in an electromagnetic–thermal manner.

B. Two-Way Approach

During the iterative process, both forward and backward, temperature and specific resistance undergo updates, respectively. In the forward iteration, electromagnetic loss is transmitted and mapped into the thermal model. Conversely, in the backward iteration, temperature is relayed to the electromagnetic model while material properties are adjusted based on the new temperature (Fig. 3). Indeed, in this method, based on the two-way

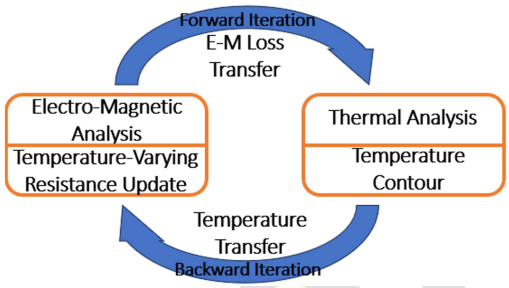

Fig. 3. Two-way electromagnetic–thermal analysis process.

coupled FEM-based software tools ANSYS Maxwell (electromagnetic analysis) and ANSYS Icepak (thermal analysis) [24], the losses are initially calculated in the electromagnetic module. The electromagnetic physics simulation of the transformer's performance incorporates temperature-dependent "bulk conductivity" for the primary and secondary copper as well as the iron core, as copper losses and eddy current losses are the dominant and main sources of heat generation in this transformer. The temperature effect on hysteresis losses is neglected.

In the first iteration, losses are calculated at all nodes and elements of the FE transformer model at ambient temperature (25 °C). Then, these losses are transferred to the thermal model of the transformer and mapped to corresponding nodes and elements. At this stage, the temperature increase of the transformer components and the surrounding air is determined based on the transferred power losses, and the thermal characteristics of the components are established. The calculated temperature is then transferred and mapped to the corresponding nodes and elements in the electromagnetic module. In this module, the electromagnetic properties of materials, including bulk conductivity, are updated based on the new temperature, and electromagnetic analysis and loss calculation are performed again at the new temperature. In the next iteration, the newly calculated losses are transferred back to the thermal module and mapped to corresponding nodes and elements. The thermal module recalculates and updates the component temperatures based on these updated power losses and transfers the new temperatures to the electromagnetic module. This process continues until the electromagnetic (current, voltage, magnetic field, and losses) and thermal (temperature) values converge within an acceptable range.

The methodology followed relies on the "temperature-dependent electrical resistance" inherent to the material properties of the transformer components: windings (copper), core (steel), and load (lead). In the proposed model, the material properties of the welding connection spot are differentiated based on the operational phases: during the welding operation period (when electrodes are connected), the properties are set to emulate lead; during the rest period (when electrodes are opened), they are modeled to simulate air.

C. Multiphysics Simulation

Based on the proposed FE analysis, the RSW transformer electrical–magnetic–thermal performance has been accessed

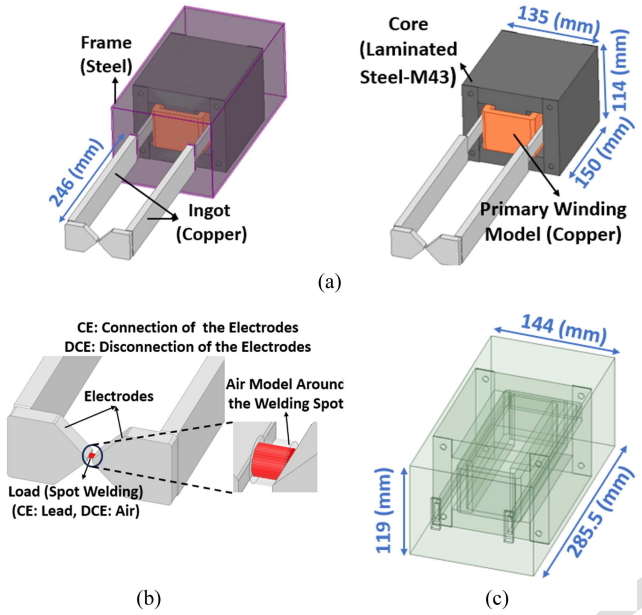

Fig. 4. RSW transformer model: (a) transformer components; (b) welding spot load; and (c) resin mold of the transformer.

through a multiphysics approach. The welding voltage, referred to as the "electrical field," is applied to the primary winding for varying cycle numbers and firing angle values. Simultaneously, via the "magnetic field" interface, this voltage induces a response in the secondary copper ingot. When the electrodes are connected, this leads to the circulation of a current across the ingot, generating the necessary heat, termed the "thermal field," for welding. Consequently, in each iteration, electromagnetic and thermal values corresponding to the new temperature, current, and voltage are determined. The 3-D modeling, components, and characteristics of the RSW transformer are illustrated in Fig. 4. The resin mold containing the transformer is meticulously modeled to ensure that the thermal simulation accurately reflects real and practical conditions, taking into account the thermal properties of the resin.

III. Proposed FEM-Based Multiphysics Approach for Determining the Steady-State Characteristics

A. Basis of the Electromagnetic–Thermal Interaction

In the RSW system, the principles of electromagnetic–thermal energy conversion follow the common (1) to (6). Based on Fig. 1

$$V_s = R_1\, I_S + L_1 \frac{dI_S}{dt} + e_1 \tag{1}$$

$$V_L = -R_2 I_L - L_2 \frac{dI_L}{dt} + e_2,\ e_1 = n e_2,\ V_L = R_L\, I_L \tag{2}$$

$$I_L\ (t) = \frac{\sqrt{2}U}{Z}\left[\sin(\omega t + \alpha - \varphi) - e^{-\frac{\omega t}{\tan\varphi}} \sin(\alpha - \varphi)\right] \tag{3}$$

$$I_{L,\text{rms}} = \frac{\sqrt{2}U}{Z} \times \sqrt{\left[\frac{1}{2} + \frac{1}{\pi}\tan(\varphi)\,\sigma\,(1 - e^{-\xi})\,(e^{\xi}\sigma - \sin(\varphi)\cos(\alpha)\right]} \tag{4}$$

$$Q = R_L\, I^2_{L,\text{rms}} t_{\text{weld}},\ t_{\text{weld}} = NT,\ T = 1/f \tag{5}$$

$$\rho c \frac{\partial T}{\partial t} = \frac{\partial}{\partial x}\left(k\frac{\partial T}{\partial x}\right) + \frac{\partial}{\partial y}\left(k\frac{\partial T}{\partial y}\right) + \frac{\partial}{\partial z}\left(k\frac{\partial T}{\partial z}\right) + Q \tag{6}$$

where V_s, V_L, I_S, I_L, e_1, e_2, and n are source voltage, load voltage, source current, load current, induced voltage in the primary winding, the induced voltage in the secondary ingot, and the transformer turns ratio, respectively, in (3) [16], U is the root mean square (rms) value of the fundamental sinusoidal source voltage on the load side, $Z = R + jL$, L and R are the equivalent inductance and resistance, respectively, $\omega = 2\pi f$ is the fundamental angular frequency, f is the frequency of the fundamental sinusoidal source voltage, t is the time, α is the firing angle, $\varphi = \omega L/R$ is equal to the phase difference between the input voltage and the corresponding current and represents the power factor (PF) angle; $I_{L,\text{rms}}$ is the rms value of I_L, $\sigma = \sin(\alpha - \varphi)$, and $\xi = \frac{2\pi}{\tan(\varphi)}$; Q is the internal heat energy of the welding resistance load; and N is the number of welding voltage cycles. Equation (6) is the heat transfer equation [8], where ρ, c, T, t, k, and (x, y, z) are the material density, specific heat capacity, temperature, time, thermal conductivity, and spatial components of the cartesian coordinate system, respectively. According to these equations, the model, boundary conditions, and electric–magnetic–thermal fields are discretized and a multiphysics analysis is performed based on FEM.

B. The Proposed FEM-Based Approach

To achieve the main study objective of evaluating the steady-state temperature of the transformer, a critical step involved aligning the temperature characteristic of the load at the welding spot [depicted in red in Fig. 4(b)] within a welding cycle of a battery strap with a "constant temperature." This determined constant temperature was carefully set to ensure a comparable temperature increase in the transformer, matching the temperature rise experienced throughout the entire welding cycle—from prewelding through welding and into the postwelding rest period. Indeed, this "equivalent constant temperature (ECT)" at the welding spot serves as a thermal source, generating a temperature increase that matches the temperature rise induced by the time-dependent temperature characteristic of the real (practical) welding cycle in the transformer.

During the welding process of each battery strap, a series of steps are performed. First, the temperature of the lead at the welding point is gradually raised until it reaches the melting point (prewelding). Subsequently, the lead is melted at the melting point (welding). Finally, the electrodes are separated, and the temperature is reduced (postwelding). The sequential repetition of this process for each battery strap leads the transformer to reach its steady-state temperature. However, achieving the steady-state temperature necessitates a real-time multiphysics transient simulation spanning several hours. Conducting such

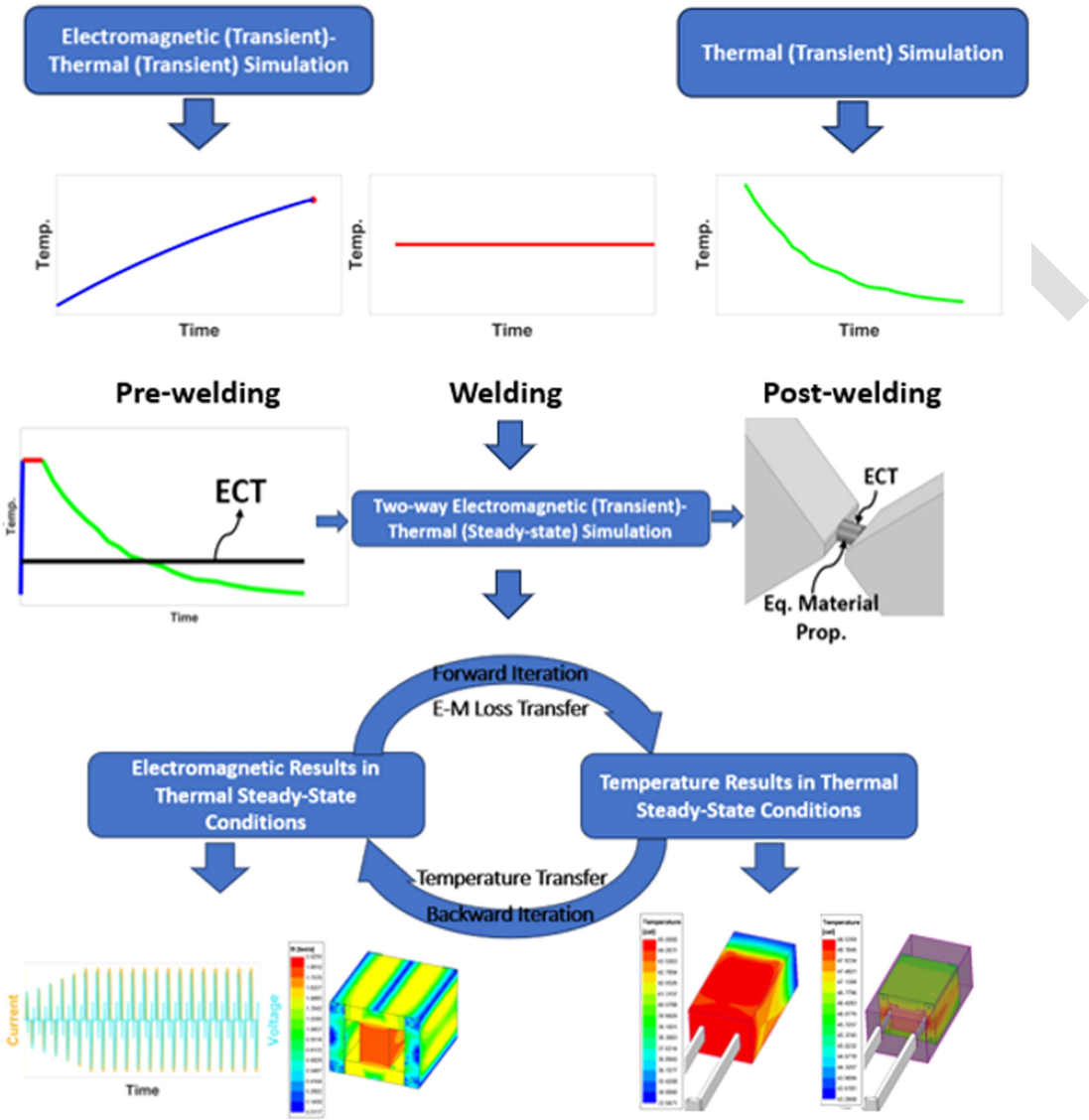

Fig. 5. Proposed FEM-based multiphysics approach for determining the steady-state characteristics of the RSW transformer.

a two-way electromagnetic (transient)–thermal (transient) simulation with a time step at the microseconds or, at most, milliseconds scale, consumes an excessive amount of time and computational resources, making it practically unfeasible or highly inefficient.

To address this challenge, the proposed methodology introduces an innovative technique based on an ECT. This technique aims to "equalize" the complete three-stage welding process for each battery strap, encompassing prewelding, welding, and postwelding. Through the utilization of the ECT, the intricate and multiphysics nature of the RSW performance is effectively "simplified." The ECT, which represents the thermal equivalent of the repetitive welding process, has been employed in the analysis of the two-way electromagnetic (transient)–thermal (steady-state) simulation. Consequently, the electromagnetic and temperature characteristics have been obtained in thermal steady-state conditions. The proposed FEM-based multiphysics approach for determining the steady-state characteristics of the RSW transformer is illustrated in Fig. 5. The subsequent sections provide a comprehensive and detailed description of this innovative approach.

IV. Three-Stage Temperature Characteristics and Its Equivalent Constant Temperature

This section presents the proposed approach and methodology for acquiring the three-stage temperature profile during battery strap welding, along with its ECT. In the battery strap welding process using these types of transformers, typically, the necessary thermal energy for melting the strap is provided with a trigger command of 35% (117°). However, considering the specifications of the battery strap welding spot, the current and frequency level of these transformers, as well as operators' experience in assessing the quality of the welding spot in practice and on the battery production line, the firing angle for a new transformer is typically set between 40% and 55% (81° to

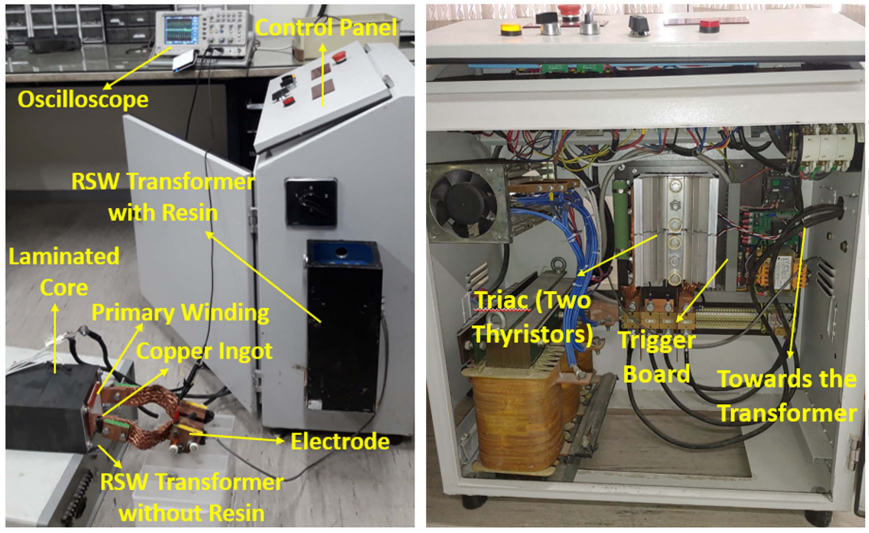

Fig. 6. Experimental test setup. (a) Test setup for RSW transformer. (b) Control panel components.

104.4°). Over time, as the transformer's performance declines due to factors, such as the deposition of scales in the cooling pipes and the degradation of insulation laminations due to heat, the firing angle may increase up to 60% (72°).

Hence, for the validation of the 3-D model of the transformer and its FEM analysis, simulation results were initially compared with experimental values for a firing angle of 30% (firing angle of 126°). The reason for this is that in the battery strap welding production line it is not feasible to use an oscilloscope for extracting voltage and current signals. Consequently, an RSW transformer was tested in the laboratory. Furthermore, aiming for repetitive usage and preventing battery strap welding in the test setup, a maximum firing angle of 30% has been employed for the excitation voltage. In this regard, in the test setup, a voltage supply of 20 cycles has been applied to the transformer. The concluding second 15 cycles consist of cutoff cycles with a firing angle of 30% of the sinusoidal supply voltage (firing angle of 126°), which has a frequency of 50 Hz and an effective value of 400 V_{rms}. The initial cycles encompass five incremental ramps with a consistent pitch. In the investigated production line, decreasing ramps are not employed at the end of the voltage cycles. The laboratory test setup and the comparison of simulation and experimental results are illustrated in Figs. 6 and 7, respectively.

As illustrated in Fig. 7, for the same input voltage, the simulated input current closely tracks the experimental input current, validating the accuracy of the FEM-based modeling and simulation. In addition, as another validation for the voltage and current results in the proposed FEM-based physics modeling and simulation approach, the PF of the transformer has been calculated and compared with the values of [6]. In [6], the PF of single-phase RSW transformers has been investigated, and a similar equivalent circuit to the one used in this article has been employed (Fig. 1). The calculated PF values for two firing angles in this article, 40% (108°) and 50% (90°), are 0.64 and 0.72, respectively, based on the following equations. These values are

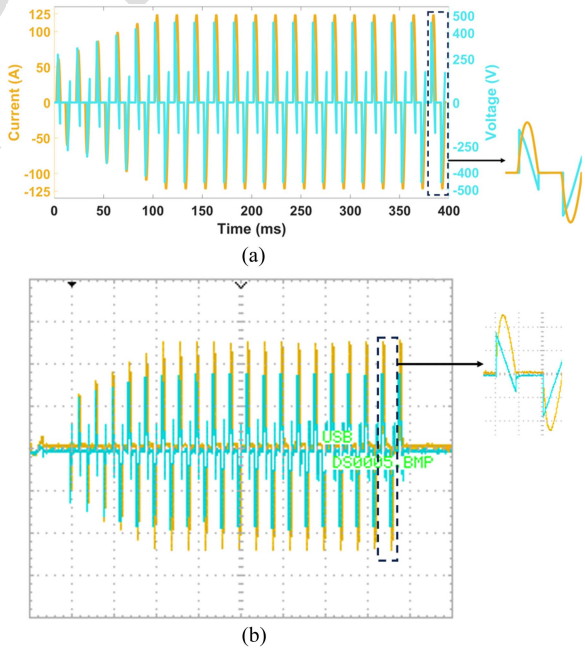

Fig. 7. Input voltage (blue) and input current (yellow) of the transformer at a frequency of 50 Hz and firing angle of 30%: (a) simulation and (b) experimental (each division on the oscilloscope corresponds to 250 V/50 A).

consistent with [6], which provides maximum values of 0.62 and 0.70 for firing angles of 117° and 81°, respectively

$$P_S\ (t)\ = V_S\ (t)\ .I_S\ (t) \tag{7}$$

$$S_S = V_{S,\text{rms}}\ .I_{S,\text{rms}} \tag{8}$$

$$\text{PF} = \frac{P_{S,\text{ave}}}{S_S} \tag{9}$$

where $P_S(t)$ and $P_{S,\text{ave}}$ are input instantaneous active power and its average value, respectively; $V_S(t)$ and $I_S(t)$ are the instantaneous input voltage and current, respectively, $V_{S,\text{rms}}$ and

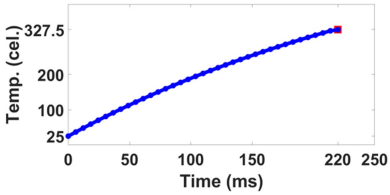

Fig. 8. Temperature characteristic of the welding load (the welding lead) during the prewelding period at a firing angle of 40% (108°).

$I_{S,\mathrm{rms}}$ are their corresponding rms values, respectively; and S_S and PF are input apparent power and PF, respectively.

In the following, the temperature characteristic and its ECT have been derived for a total of 20 cycles of the supply voltage. The fundamental sinusoidal supply voltage is 400 V_{rms} at a frequency of 50 Hz. The 15 cycles are obtained with a 40% firing angle (firing angle of 108°). The first five cycles consist of a uniform incremental ramp waveform with a consistent step. Simulations have been executed for an ambient temperature of 25 °C.

A. Prewelding

This initial stage commences with electrode connection and current establishment. The battery strap lead, initially at ambient temperature, is positioned between the electrodes, gradually increasing in temperature until reaching the melting point of lead (327.5 °C). The prewelding temperature profile of the welding spot (the welding lead) is derived through electromagnetic (transient)–thermal (transient) analysis.

By applying the welding voltage to the primary winding of the transformer, the temperature characteristic of the welding lead has been determined through the transient electrical–magnetic–thermal simulation based on the "temperature-dependent electrical resistance."

In Fig. 8, the profile of the welding load (the welding spot) temperature increase during the prewelding stage is illustrated. In this figure, the temperature represents the volumetric average temperature of the welding load (the welding spot) at each moment. The characteristic of temperature rise during prewelding has been illustrated in Fig. 9. After 220 ms of electrode contact and current passing through, the entire welding lead has reached the melting point temperature.

B. Welding

At this stage, after the welding lead reaches the melting point during the prewelding phase, the energy received from the source is utilized in a constant temperature process (at the melting point of lead) for melting and consequently welding. In this manner, the molten lead (weld nugget) continues to grow until complete melting occurs, leading to the formation of a spot weld [Fig. 10(a)].

In this characteristic, due to the small size of the welding solder and the short welding time (especially during the prewelding period), any temperature increase of the solder beyond its melting temperature has been neglected.

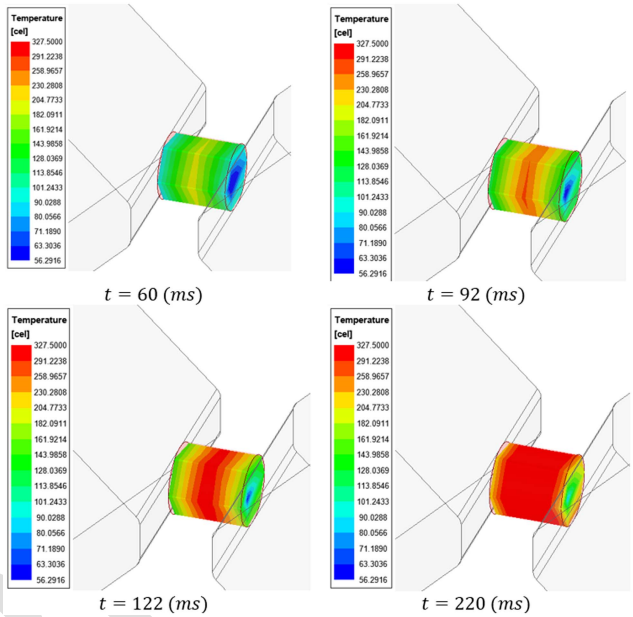

Fig. 9. Characteristic temperature contour of the welding lead during the prewelding period at a firing angle of 40%.

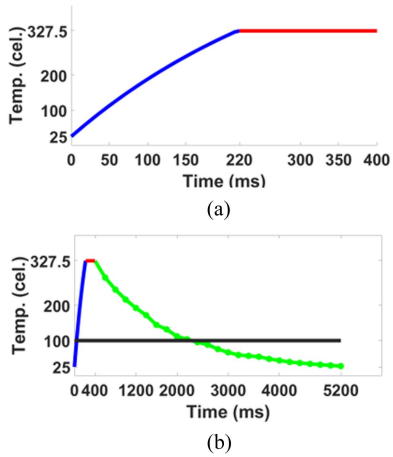

Fig. 10. Characteristic temperature of the welding spot and its ECT. (a) Characteristic temperature of the welding lead during the prewelding (blue) and welding (red) period for the 20 welding voltage cycles at the firing angle of 40%. (b) Temperature characteristic of the welding spot (between the electrodes) during a complete welding cycle of a battery strap for 20 cycles at a 40% firing angle voltage: prewelding (blue), welding (red), postwelding (green), and ECT (black).

In addition, the heat required to raise the temperature of lead from 25 °C to its melting point (327.5 °C) and the heat required for the solid-to-liquid transformation at the melting temperature are calculated to be 23 and 39 m joules, respectively, where m represents the mass of lead in grams, considering the specific heat capacity and latent heat of lead. Therefore, considering the ratio between these two energies and the time ratio of 220 (start of complete nugget formation) to 400 ms (end of energy application), it becomes evident that the available time for raising the temperature of molten lead beyond its melting point is limited and negligible. For longer durations of energy

application (e.g., 30 cycles: 600 ms), it is possible to consider an increase in the temperature of the molten lead beyond its melting point.

C. Postwelding

After completing the battery strap welding, the electrodes are separated and the current is interrupted. The time interval between electrode separation and their reconnection for the next battery strap welding is the postwelding or rest period, during which air is present between the electrodes. To determine the temperature profile of the welding spot (between the electrodes), it is necessary to establish the temperature characteristics of the air between the electrodes during postwelding. To determine the temperature characteristic of the rest period, the proposed approach suggests considering the average temperature of the air around the welding spot during each time interval as the temperature of the welding spot (air between the electrodes) in the subsequent time interval. The concept underlying this approach revolves around the thermal interchange between the ambient air surrounding the electrodes and the air present between them. In the last instance of electrode connection during the welding process (t_0), the molten lead (at its melting temperature T_0) is placed between the electrodes. At this specific moment, the average temperature of the ambient air surrounding the welding spot is computed (T_1) within a volume equal to the volume of the welding spot [Fig. 4(b)] in a transient thermal analysis. The temperature profile of the welding spot during the electrode connection period [Fig. 10(a)] has been considered as the input for this analysis, corresponding to the time interval of $[0, t_0]$.

In the subsequent step where the electrodes are separated, the temperature T_1 (the temperature of the surrounding air at the welding spot in the previous stage) is considered as the temperature of the welding spot between the electrodes (now consisting of air). This approach is based on the assumption that after the separation of the electrodes, the surrounding air at the welding spot (between the electrodes) is drawn into this point (spot). In this step, the average temperature of the ambient air surrounding the welding spot (T_2) has been determined. The input applied to the welding spot in the thermal analysis of this stage comprises temperature values within the range of $[0, t_1]$. This includes the temperature characteristic of the solder during the electrode joining period, ranging from $[0, t_0]$, and the temperature characteristic of the air between the electrodes, ranging from $[t_0, t_1]$. Taking into account the displacement and heat transfer between the air within the welding spot (between the electrodes) and the surrounding air, T_2 is regarded as the temperature of the air at the welding spot in the subsequent stage. This methodology has been pursued until the end of the postwelding (rest period). The implementation of this approach is depicted in Fig. 11 and Table I for a 4.8 s rest period, providing a visual representation of the process. Therefore, the temperature reduction characteristic during the postwelding has been established. The postwelding temperature characteristic is illustrated in Fig. 10(b). At the end of the postwelding, the welding spot temperature has nearly reached the ambient temperature.

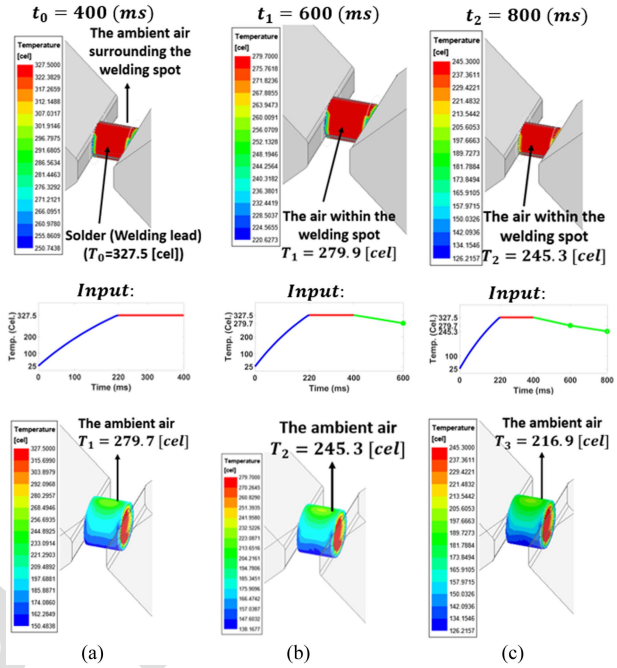

Fig. 11. First three steps of determining the temperature of the air at the welding spot (between the electrodes) during the postwelding stage. Determination of (a) T_1; (b) T_2; and (c) T_3 (also see Table I).

TABLE I
TEMPERATURE OF THE AIR INSIDE AND SURROUNDING THE WELDING POINT DURING POSTWELDING IN °C FOR 20 WELDING CYCLES AND A RESTING PERIOD OF 4.8 S (ALSO SEE FIG. 11)

Time(ms)	400	600	800	…	4800	5000	5200
T^{sw}	327.5*	279.7	245.3	…	31.2	29.2	27.3
T^{amb}	279.7	245.3	216.9	…	29.2	27.3	25.5

T^{sw}: The average temperature of the welding spot.
T^{amb}: The average temperature of the ambient air surrounding the welding spot.
*: This temperature is the molten lead temperature at the welding spot in the final moment of welding. The other temperatures listed in the table represent the temperature of the air inside or surrounding the welding spot.
Time $= t_i$, $T^{sw} = T_i$, $T^{amb} = T_{i+1}$, $i = 0,1,2,\ldots,24$.

D. Equivalent Constant Temperature (ECT)

The temperature characteristic of the welding spot [Fig. 10(b)] presents the thermal behavior of this region (between the electrodes) during a complete welding cycle of a battery strap. The periodic repetition of this characteristic in consecutive welding of battery straps, accompanied by the temperature rise resulting from the current passage (losses) in the core, windings, and copper ingot, brings the transformer (especially the transformer frame and core) to a steady-state temperature. Achieving the steady-state temperature in transient thermal analysis requires conducting an extensive sequence of consecutive welding cycles, equivalent to several hours of real-time, through multiphysics simulations. However, this computational method demands an exceedingly high amount of computational resources and time, making it nearly unfeasible or highly inefficient. Moreover, because of the time-dependent nature of the welding temperature characteristic, it cannot be directly integrated into steady-state thermal analysis for multiphysics

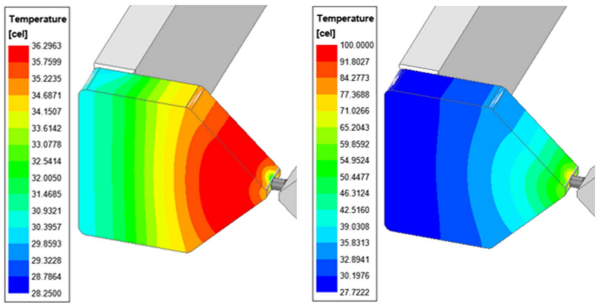

Fig. 12. Rise in electrode temperature for 20 cycles at a 40% firing angle voltage due to: (a) actual temperature characteristic at the welding spot; and (b) ECT = 100.1 [Cel.].

simulations. To overcome this challenge, the proposed approach in this article is the ECT method. The ECT of the welding spot is determined in a way that the resulting temperature increase in the transformer matches the actual temperature rise caused by the welding spot's characteristic temperature [Fig. 10(b)]. In fact, the basis of this method is to ensure that ECT generates the same temperature increase in the transformer as the sequence of actual temperature characteristics within a specified time interval. Consequently, it can be expected that with an appropriate approximation, the steady-state temperature of transformer in simulation, using the ECT, closely approximates the actual steady-state temperature of the transformer.

In a transient single-physics thermal analysis, multiple sequential welding temperature profiles are applied to the welding spot, and the resulting temperature increase in the transformer (especially in the electrodes) is extracted. Simultaneously, the ECTs are applied to the welding spot within the same time interval. The ECT that yields a temperature increase close to the temperature increase of the sequential temperature profiles in the transformer is considered as a substitute equivalent thermal source. The equivalent thermal source is positioned between the electrodes. Its material, thermal properties, temperature (ECT), and electromagnetic properties are modeled in a way that ensures it is equivalent to the real thermal and electromagnetic conditions. In other words, this modeling approach simplifies the complicated and multiphysics welding process, which involves material and phase transitions (during electrode contact, the material between them is solid and molten lead, while during electrode separation, the material between them is air), by providing an equivalent representation at the welding spot. The thermal properties of the source material have been considered equivalent to the thermal properties of air [since the duration of electrode separation during continuous welding (postwelding) is longer than the duration of electrode contact]. Additionally, its electromagnetic properties have been modeled based on the electromagnetic properties of lead (as lead is located between the electrodes during electrode contact and transformer electromagnetic performance).

As an example, consider Fig. 12, which illustrates the contour and average increase in electrodes temperature for one welding

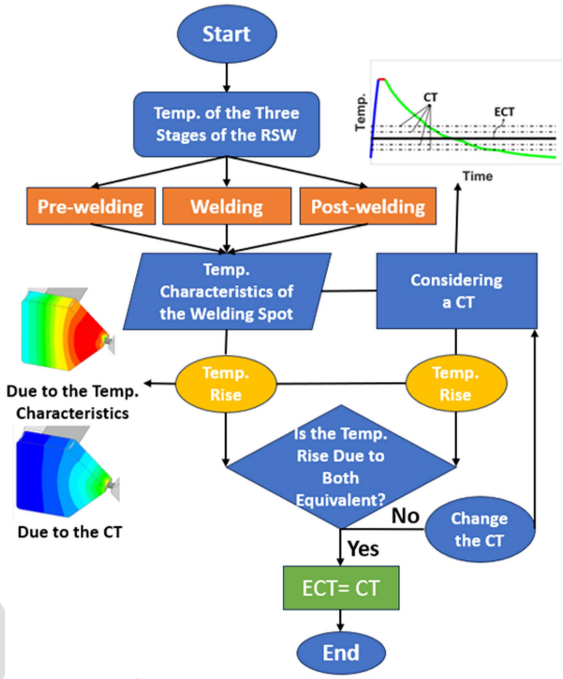

Fig. 13. Process of obtaining ECT (CT: a constant temperature).

TABLE II
ECT IN °C CORRESPONDING TO DIFFERENT WELDING CONDITIONS (FIRING ANGLE, REST PERIOD, AND NUMBER OF INPUT VOLTAGE CYCLES)

Firing angle	Rest period (s)	20 cycles	30 cycles
40% (108°)	**3.8**	111.3	137.1
	4.8	100.1	123.7
	5.8	91.6	113.7
50% (90°)	**3.8**	150.6	185.6
	4.8	135.4	167.5
	5.8	124.0	153.9

cycle, along with its corresponding ECT. The temperature rise due to the ECT closely aligns with the increase resulting from the welding temperature characteristic. The flowchart of the process of obtaining the ECT is illustrated in Fig. 13. Based on this approach, Table II shows the ECTs for different welding conditions.

V. RESULTS AND EXPERIMENTAL VALIDATION

The temperature and electromagnetic characteristics of the RSW transformer have been predicted using the two-way electromagnetic (transient)–thermal (steady-state) analysis. The material between the electrodes is modeled using an equivalent material at a constant temperature (the ECT) as discussed in the previous section. The temperature of the remaining components, such as the core, windings, and copper ingot, also increases based on the "temperature-dependent electrical resistance" concept. The cooling effect of water-cooling pipes has been applied as boundary conditions on the surface of the copper ingot in the simulation. This is due to the fact that both the cooling pipe and the ingot (transformer's secondary) material are made of copper (the boundary material is unchanged), and the water temperature

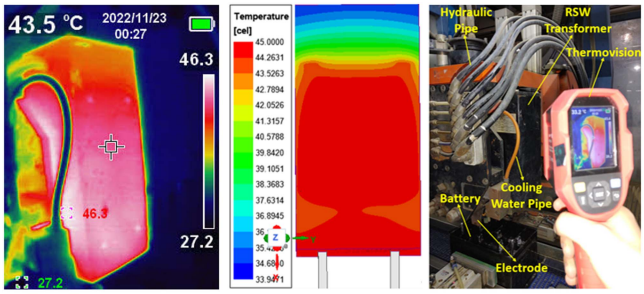

(a) (b) (c)

Fig. 14. Steady-state temperature of the RSW transformer frame for an input of 20 voltage cycles with a firing angle of 40% and a rest period of 4.8 s: (a) experimental; (b) simulation; and (c) components in the welding line.

inside the pipe connected to the large source remains nearly constant with minimal changes, always equal to the ambient equilibrium temperature (Fig. 14).

In each iteration of the electromagnetic–thermal simulation, the temperature and electromagnetic properties are successively updated in the electromagnetic specifications (losses) and the newly adjusted temperature, respectively. This iterative process results in the steady-state temperature of the transformer. Simulations have been executed for an ambient temperature of 25 °C.

A. *Temperature Results*

Fig. 14 illustrates the steady-state temperature of the transformer frame for an input of 20 voltage cycles with a firing angle of 40% and a rest period of 4.8 s. As observed, the simulation closely follows the experimental results, indicating the effectiveness of the proposed approach. In order to achieve a more accurate comparison between simulation and experimental results, a transformer with an identical design to previous models has been constructed, incorporating PT100 temperature sensors placed before the resin encapsulation. The steady-state temperatures of the transformer components are illustrated in Fig. 15. The term "steady-state temperature" in an electromagnetic system refers to a constant temperature that various components reach after operating for a specific duration. In this state, the temperature only exhibits minor fluctuations (Fig. 15).

One primary reason for the lower temperature in simulations compared to the experimental temperature is attributed to the omission of the higher temperatures reached by the molten lead beyond its melting point. This has been explained in Section IV-B. Another major reason for the small discrepancy is the limitation of space and time for processor analysis, which sets the simulation time step to be in the millisecond scale for two-way simulations. This results in the simulated current and voltage peaks being slightly lower than their actual values (see Appendix for more details). Another reason to consider is the fouling of the cooling water pipes. Since RSW transformers operate continuously in battery production lines, the accumulation of deposits in the pipes can lead to a reduction in cooling effectiveness over time. Hence, the temperature of the ingot at the investigated point in the simulation, assuming ideal

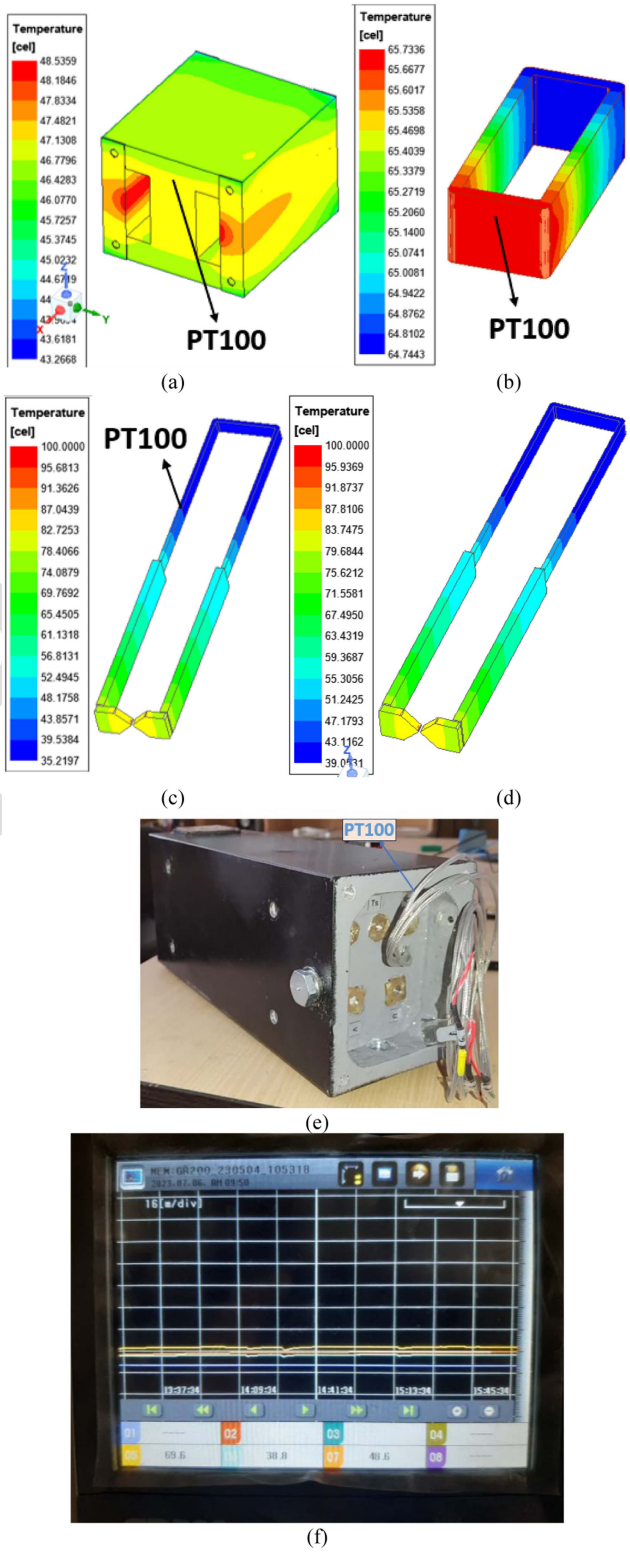

Fig. 15. Steady-state temperatures of the fabricated transformer components for an input of 20 voltage cycles with a firing angle of 40% and a rest period of 4.8 s: (a) core; (b) primary winding; (c) secondary winding (ingot) for an ideal cooling water pipe without deposits; (d) secondary winding (ingot) for the cooling water pipe with a 50% reduction in the effective cross-sectional area due to sedimentation; (e) fabricated RSW transformer, along with the incorporated PT100 temperature sensors; and (f) steady-state temperatures recorded by the PT100 sensors. Channels: primary winding (yellow), secondary winding (blue), and core (orange).

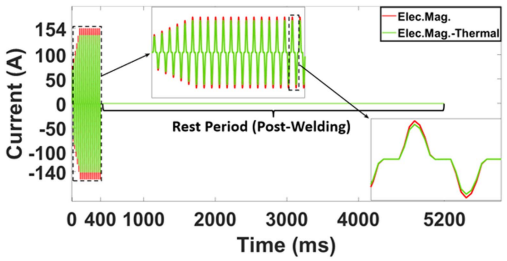

Fig. 16. Comparison of primary winding current: electromagnetic analysis (Elec.Mag.) and electromagnetic–thermal (Elec.Mag.–Thermal) analysis.

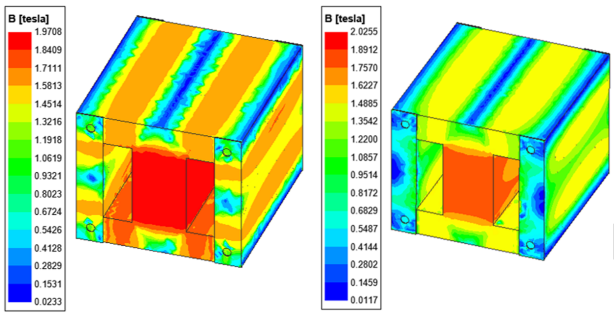

$Avg.B = 1.58\ [T]$ (a) $Avg.B = 1.38\ [T]$ (b)

Fig. 17. Maximum magnetic flux density of the transformer core: (a) electromagnetic analysis and (b) electromagnetic–thermal analysis.

and clean pipes, is 35.2 °C [Fig. 15(c)], which is lower than the corresponding experimental value of 38.8 °C. However, when considering the cooling effect associated with a roughly 50% reduction in the effective cross-sectional area of the pipe due to fouling, the temperature increases to 39 °C [Fig. 15(d)]. Therefore, this approach can also be used to predict the temperature conditions resulting from the fouling of the cooling water pipes.

B. Electrical Results

Fig. 16 illustrates the primary winding current considering the effect of steady-state temperature (electromagnetic–thermal analysis) compared to the case without considering it (only electromagnetic analysis). The reason for the lack of high smoothness in the plot is that the time step used in this simulation was in the millisecond scale. The current amplitude was reduced by 10% when accounting for the temperature effect due to the increased electrical resistance. This reduction highlights the significance of incorporating steady-state thermal analysis for accurate prediction of current and voltage. This difference becomes more pronounced at higher percentages of the firing angle, increased the number of welding voltage cycles, and shorter rest period.

C. Magnetic Results

Fig. 17 illustrates the distribution of the maximum flux density of the magnetic field of the RSW transformer core. The average flux density varies by approximately 15%. This variation can be even greater at different firing angles, number of welding voltage cycles, and rest periods. Considering that the RSW transformer core typically operates near saturation during welding, it is crucial to consider the impact of steady-state temperature on the flux density of core in transformer design.

The effect of temperature on the magnetic field of the RSW transformer core depends on the welding operating point, and it cannot generally be described by a simple direct or inverse relationship. This influence varies under different conditions, such as firing angles, number of voltage cycles, rest periods, and cooling arrangements. On the other hand, at a specific welding point with defined operating conditions, considering that an increase in temperature leads to an increase in resistance and a decrease in current, determining the voltage drop accurately, which is the difference between the supply voltage and the induced voltage in the winding, is not a straightforward path because the magnetic field in the core depends on the induced voltage created in the winding. Therefore, predicting the magnetic field in the core at a specific operating point, as proposed in this article, requires an electromagnetic–thermal analysis.

VI. Conclusion

In this article, a novel FEM-based approach was proposed to predict the temperature and electromagnetic behavior of a RSW transformer under steady-state thermal conditions. The complexity of the RSW process, with its inherent temperature dependency and involvement of phase transitions (melting) and structural changes (like electrode separation and connection), makes conventional transient and steady-state thermal analyses inadequate for determining the steady-state temperature of the RSW transformer. The proposed approach has successfully determined the temperature characteristic of the welding spot and its corresponding ECT. Leveraging the ECT alongside a two-way electromagnetic–thermal analysis, it is possible to predict and experimentally validate the temperature and electromagnetic characteristics across various power electronics parameters, such as firing angles, welding voltage cycle counts, and rest periods. These prediction capabilities hold significant potential for application in both the design and operational phases of WTs. The insights gained from these predictions offer valuable guidance for optimizing the transformer performance and efficiency. Additionally, this approach can be extended to other electromagnetic systems and processes with variable material phases and structures that are time- and temperature-dependent.

Appendix

This Appendix presents the simulation details. The number of Tetrahedral (Tet.) elements of the FE model is specified in Table III. The specifications of simulations are provided in Table IV. A personal computer was employed for running the simulations. In case of utilizing high-performance computing processors (such as cloud computing), the processing time of the simulations can be significantly reduced.

The specifications of the computer used were as follows.

1) Processor: Intel(R) Core (TM) i7-10750H CPU @ 2.60 GHz 2.59 GHz.
2) Installed RAM: 16.0 GB (15.8 GB usable).

TABLE III
MESH SPECIFICATIONS OF THE FE MODEL OF THE MAIN COMPONENTS OF THE RSW TRANSFORMER

Component	Num. tets.	RMS edge length (mm)	Min. tet. vol. (mm^3)	Max. tet. vol. (mm^3)	Mean tet. vol. (mm^3)
Core	67894	8.036	0.006	85.817	26.717
Frame	1295	50.582	5.705	2740.11	212.629
Spot welding	4150	0.529	8.426e−5	0.030	0.005
Ingot	4294	13.407	8.657e−6	6729.19	66.835
Windings	32371	5.631	0.012	30.907	7.241
Total number of elements: 143195 tets.					

TABLE IV
SPECIFICATIONS OF SIMULATIONS

Simulations	Analysis type	Time step (ms)	Execution duration (h)	Space (GB)
Voltage and current only due to Elec.Mag. analysis	Elec.Mag. (Tr)	0.2	71.0	67.8
Pre-welding	Elec.Mag. (Tr)-thermal (Tr)	1	65.8	64.0
Post-welding	Thermal (Tr)	200	2.2	34.3
ECT (for each CT)	Thermal (Tr)	200	0.7	5.4
Temp. and Elec.Mag. characteristics in thermal steady-state	Elec.Mag. (Tr)-thermal (SS)	1	562.5	464
Tr: Transient analysis. SS: Steady-state analysis. CT: Constant temperature. ECT: Equivalent constant temperature.				

3) Solver: DRS4 (in ANSYS Electronics 2021 R2).

ACKNOWLEDGMENT

This work has been accomplished at the Sun-Air Research Institute (SARI), Ferdowsi University of Mashhad, Mashhad, Iran, and has been funded by the SARI itself.

REFERENCES

[1] M. Pouranvari and S. P. H. Marashi, "Critical review of automotive steels spot welding: Process, structure and properties," *Sci. Technol. Weld. Joining*, vol. 18, no. 5, pp. 361–403, 2013.
[2] K. Zhou and P. Yao, "Review of application of the electrical structure in resistance spot welding," *IEEE Access*, vol. 5, pp. 25741–25749, 2017.
[3] W. Li, D. Cerjanec, and G. A. Grzadzinski, "A comparative study of single-phase AC and multiphase DC resistance spot welding," *J. Manuf. Sci. Eng.*, vol. 127, no. 3, pp. 583–589, 2005.
[4] S. C. A. Alfaro, J. E. Vargas, M. A. Wolff, and L. O. Vilarinho, "Comparison between AC and MF-DC resistance spot welding by using high speed filming," *J. Achievements Mater. Manuf. Eng.*, vol. 24, no. 1, pp. 333–339, 2007.
[5] P. Podrzaj, I. Polajnar, J. Diaci, and Z. Kariz, "Overview of resistance spot welding control," *Sci. Technol. Weld. Joining*, vol. 13, no. 3, pp. 215–224, 2008.
[6] K. Zhou and L. Cai, "Online measuring power factor in AC resistance spot welding," *IEEE Trans. Ind. Electron.*, vol. 61, no. 1, pp. 575–582, Jan. 2014.
[7] R. Shafaei, M. Ordonez, and M. A. Saket, "Three-dimensional frequency-dependent thermal model for planar transformers in LLC resonant converters," *IEEE Trans. Power Electron.*, vol. 34, no. 5, pp. 4641–4655, May 2019.
[8] H. M. Ahn, B. J. Lee, and S. C. Hahn, "An efficient investigation of coupled electromagnetic-thermal-fluid numerical model for temperature rise prediction of power transformer," in *Proc. Int. Conf. Elect. Mach. Syst.*, 2011, pp. 1–4.
[9] C. Liao, J. Ruan, C. Liu, W. Wen, and Z. Du, "3-D coupled electromagnetic-fluid-thermal analysis of oil-immersed triangular wound core transformer," *IEEE Trans. Magn.*, vol. 50, no. 11, Nov. 2014, Art. no. 8401904.
[10] J. Smolka and A. J. Nowak, "Experimental validation of the coupled fluid flow, heat transfer and electromagnetic numerical model of the medium power dry-type electrical transformer," *Int. J. Thermal Sci.*, vol. 47, no. 10, pp. 1393–1410, 2008.
[11] A. Lefèvre, L. Mièggeville, J. Fouladgar, and G. Olivier, "3-D computation of transformers overheating under nonlinear loads," *IEEE Trans. Magn.*, vol. 41, no. 5, pp. 1564–1567, May 2005.
[12] C. Li, J. Chen, C. Xue, Z. Liu, and P. Davari, "Simultaneous multispot temperature prediction of traction transformer in urban rail transit using long short-term memory networks," *IEEE Trans. Transp. Electrific.*, vol. 9, no. 3, pp. 4552–4561, Sep. 2023.
[13] A. Abdali, A. Abedi, K. Mazlumi, A. Rabiee, and J. M. Guerrero, "Novel hotspot temperature prediction of oil-immersed distribution transformers: An experimental case study," *IEEE Trans. Ind. Electron.*, vol. 70, no. 7, pp. 7310–7322, Jul. 2023.
[14] M. Ngo, Y. Cao, D. Dong, R. Burgos, K. Nguyen, and A. Ismail, "Forced air-cooling thermal design methodology for high-density, high-frequency, and high-power planar transformers in 1U applications," *IEEE J. Emerg. Sel. Topics Power Electron.*, vol. 11, no. 2, pp. 2015–2028, Apr. 2023.
[15] H. Eisazadeh, M. Hamedi, and A. Halvaee, "New parametric study of nugget size in resistance spot welding process using finite element method," *Mater. Des.*, vol. 31, no. 1, pp. 149–157, 2010.
[16] K. Zhou and H. Li, "A comparative study of single-phase AC and medium frequency DC resistance spot welding using finite element modeling," *IEEE Access*, vol. 8, pp. 107260–107271, 2020.
[17] Y. J. Xia, T. L. Lv, H. Ghassemi-Armaki, and Y. B. Li, "Collaborative simulation of nugget growth and process signals for resistance spot welding," *Weld. World*, vol. 67, no. 6, pp. 1377–1392, 2023.
[18] M. Eshraghi, M. A. Tschopp, M. A. Zaeem, and S. D. Felicelli, "Effect of resistance spot welding parameters on weld pool properties in a DP600 dual phase-steel: A parametric study using thermomechanically-coupled finite element analysis," *Mater. Des.*, vol. 56, pp. 387–397, 2014.
[19] V. H. Baltazar Hernandez, M. L. Kuntz, M. I. Khan, and Y. Zhou, "Influence of microstructure and weld size on the mechanical behaviour of dissimilar AHSS resistance spot welds," *Sci. Technol. Weld. Joining*, vol. 13, no. 8, pp. 769–776, 2008.
[20] H. Zhigang, W. Yuanxun, L. Chunzhi, and C. Chuanyao, "A multi-coupled finite element analysis of resistance spot welding process," *Acta Mechanica Solida Sinica*, vol. 19, no. 1, pp. 86–94, 2006.
[21] H. S. Cho and Y. J. Cho, "A study of the thermal behavior in resistance spot welds," *Weld. J.*, vol. 68, no. 6, pp. 236–244, 1989.
[22] K. S. Yeung and P. H. Thornton, "Transient thermal analysis of spot welding electrodes," *Weld. J.*, vol. 78, no. 1, pp. 1–6, 1999.
[23] J. A. Khan, L. Xu, and Y. Chao, "Prediction of nugget development during resistance spot welding using coupled thermal-electrical-mechanical model," *Sci. Technol. Weld. Joining*, vol. 4, no. 4, pp. 201–207, 1999.
[24] *ANSYS Electronics Reference Manual*, v. R2, 2021.

Armin Saki was born in Khorramabad, Iran, on 25 January 1994. He received the diploma degree (Hons.) from the Sampad Schools affiliated to the National Organization for the Development of Exceptional Talents, Tehran, Iran, the B.Sc. degree in electrical power engineering from the Shahid Chamran University of Ahvaz, Ahvaz, Iran, in 2016, and the M.Sc. degree in electrical power engineering from the University of Isfahan, Isfahan, Iran, in 2019. He is currently working toward the Ph.D. degree (Hons.) in electrical power engineering with the Ferdowsi University of Mashhad, Mashhad, Iran.

His research interests include the design and optimization of electrical machines and multiphysics, and vibroacoustic and thermal analysis of them, based on FEM.

Saleh Rahmani was born in Mashhad, Iran, on 11 November 1989. He received the B.Sc. degree in electrical power from the Industrial University of Shahrood, Shahrud, Iran, in 2012, and the M.Sc. degree in electrical power engineering, the trend of electrical machine from the Shahed University of Tehran, Tehran, Iran, in 2015.

His research interests include the design and optimization of electrical machines and design and manufacturing of battery charging and testing devices.

Masoud Yavarinasab was born in Mashhad, Iran, on 25 June 1985. He received the B.Sc. degree in power electrical, in 2009, and the M.Sc. degree in energy engineering, in 2012.

He is working as the Head of Energy Storage Systems and Power Electronics with the Sun Air Research Institute, Ferdowsi University of Mashhad, Mashhad, Iran. His research interests include renewable energy, energy storage, lithium batteries, and power electronics.

Hossein Abootorabi Zarchi (Senior Member, IEEE) received the M.S. and Ph.D. degrees in electrical engineering from the Isfahan University of Technology, Isfahan, Iran, in 2004 and 2010, respectively.

He was a Visiting Ph.D. Student with the Control and Automation Group, Denmark Technical University, Kongens Lyngby, Denmark, from 2009 to 2010. He is currently an Associate Professor with the Department of Electrical Engineering, Ferdowsi University of Mashhad, Mashhad, Iran. His research interests include electrical machines and drives, nonlinear control of motor drives, and renewable energies.

Salman Abdi (Senior Member, IEEE) received the B.Sc. degree in electrical engineering from the Ferdowsi University, Mashhad, Iran, in 2009, the M.Sc. degree in electrical engineering from the Sharif University of Technology, Tehran, Iran, in 2011, and the Ph.D. degree in electrical machines design and optimization from the Cambridge University, Cambridge, U.K, in 2015.

He is currently an Assistant Professor in electrical engineering with the University of East Anglia, Norwich, U.K. His research interests include electrical machine design, modeling, and instrumentation for renewable power generation and electric propulsion systems.

Sérgio M. A. Cruz (Senior Member, IEEE) received the diploma, M.Sc., Dr.Eng. degrees in electrical engineering from the University of Coimbra, Coimbra, Portugal, in 1994, 1999, and 2004, respectively.

He has been with the Department of Electrical and Computer Engineering, University of Coimbra, where he is currently an Associate Professor with the Habilitation and the Director of the Electric Machines Laboratory. His research interests include power transformers, rotating electric machines, electric drives, and power electronic converters, with special emphasis on fault diagnosis, fault tolerance, and digital control.

Hamidreza Mosaddegh-Hesar (Member, IEEE) received the Ph.D. degree in electrical engineering from the Ferdowsi University of Mashhad, Mashhad, Iran, in 2020.

He is currently a Postdoctoral Fellow with the École de technologie supérieure, Montreal QC, Canada. His research interests include control of high-performance drives, modeling of electrical machines, and renewable energies.

Dr. Mosaddegh-Hesar is an Associate Editor for IEEE TRANSACTIONS ON INDUSTRY APPLICATIONS.